







Neuro-adaptive backstepping integral sliding mode control design for nonlinear wind energy conversion system

Imran ULLAH KHAN¹ , Laiq KHAN^{1,*} , Qudrat KHAN² , Shafaat ULLAH¹ ,
Uzair KHAN¹ , Saghir AHMAD¹ 

¹Department of Electrical and Computer Engineering, COMSATS University Islamabad, Abbottabad Campus, Abbottabad, Pakistan

²Center for Advanced Studies in Telecommunication, COMSATS University Islamabad, Islamabad, Pakistan

Received: 23.01.2020

Accepted/Published Online: 29.07.2020

Final Version: 30.03.2021

Abstract: The electrical power extracted from a wind energy conversion system (WECS) tends to be inconsistent due to the intermittent nature of the wind. This issue is addressed by formulating a maximum power point tracking (MPPT) control strategy that optimizes the power extraction from the WECS under a wide range of wind speed profiles. This research article focuses on the formulation of a nonlinear neuro-adaptive backstepping integral sliding mode control (NABISMC) based MPPT strategy for a standalone, variable speed, fixed-pitch WECS equipped with a permanent magnet synchronous generator (PMSG). The proposed paradigm is a hybrid of the conventional backstepping and the integral sliding mode control (ISMC) based MPPT schemes. The effectiveness of the control strategy devised is guaranteed through numerical simulations carried out in Matlab/Simulink for a 3 kW PMSG-WECS under a stochastic wind speed profile. Further validation is guaranteed by giving a detailed performance comparison analysis of the proposed MPPT control strategy with the conventional feedback linearization control (FBLIC), proportional integral derivative (PID) control, sliding mode control (SMC), and standard neuro-adaptive integral sliding mode control (NAISMC) based MPPT strategies, where the proposed strategy is found superior to all the stated strategies in terms of offering more accurate MPPT, lower steady state error, faster dynamic response and lesser chattering.

Key words: Wind energy conversion system (WECS), permanent magnet synchronous generator (PMSG), maximum power point tracking (MPPT), variable speed wind turbine (VSWT), backstepping, integral sliding mode control (ISMC), feedforward neural network

1. Introduction

The worldwide growing energy demand has urged the investigation of cost competitive, environment-friendly and renewable energy sources to supplement the conventional nonrenewable energy sources for electricity generation. Due to rapid increase in the worldwide installed capacity and the advancement in the wind turbine size and design, the wind energy is regarded as the mature technology and fastest growing among all the other renewable energy sources [1].

Over the past decade, when compared with its fixed-speed counterparts, the variable speed wind turbine (VSWT) has undergone through a fast development and has proved itself the industry standard. This is characterized by its high power conversion efficiency and delivering a better quality of electric power [2]. In general, due to the variability of the wind speed, the wind energy conversion system (WECS) exhibits variation

*Correspondence: laiq@cuiatd.edu.pk

in its electric power output. This makes the inherent characteristics of the WECS nonlinear; thus, making the maximum power extraction a challenging task. For maximizing the efficiency of a WECS, the formulation of an MPPT control strategy plays a key role [3, 4].

The literature reveals that different categories of electric generators have been employed in WECS with power ratings upto several MWs, comprising squirrel cage induction generator (SCIG), doubly fed induction generator (DFIG), wound rotor synchronous generator (WRSG) and permanent magnet synchronous generator (PMSG). Among these stated categories, the PMSG is preferred for a variable speed WECS due to its higher power density, higher efficiency, higher power factor, lower maintenance cost, lack of excitation and gear-box, and a wide operating speed range (0%–100%) [5, 6].

Significant amount of research has been conducted for optimizing the power extraction from a WECS. Different MPPT control strategies have been formulated in the literature. Most of the strategies have focused on the formulation of nonlinear MPPT techniques. One of the most promising robust nonlinear MPPT control strategies is the sliding mode control (SMC). The SMC renders several attractive features, such as simple design, fast dynamic response, insensitivity to parametric variations and disturbance rejection. From these stated attributes, apparently the SMC scheme seems an ideal solution for MPPT, nevertheless, the occurrence of the chattering phenomenon as well as the asymptotic convergence, because of a linear sliding surface in the first order SMC, invites a high level of criticism. The chattering phenomenon forces the system response to oscillate around the sliding surface (desired reference), thus, causing a higher mechanical wear and tear, poor tracking performance and overheating of the power circuits [7–11]. In the context of the conventional SMC, the system robustness against parametric variations and external disturbances is guaranteed only during the sliding phase, but not during the reaching phase. Moreover, the order of the motion equation during the sliding phase equals $n - m$, where n represents the dimension of the state space, while m indicates the dimension of the control input. In other words, the order of the motion equation in case of the conventional SMC is reduced by the dimension of the control input. To counteract these stated issues, an integral sliding mode control (ISMC) scheme has been proposed in [12]. In the ISMC strategy, chattering is alleviated by removing the discontinuous control signal from the original control path and inserting it into the internal dynamic process for generating the sliding mode. Starting from the initial time instance, the sliding phase (robustness of the system) is guaranteed throughout the system response. The order of the motion equation equals the original system state space dimension, and it is not reduced by the dimension of the control input. Moreover, smaller maximum control magnitude is required for the ISMC than the conventional SMC, since the value is usually bigger during the reaching phase. However, the main problem with the standard ISMC is the difficulty of tuning its switching gain parameter in order to have a good balance between the disturbance rejection property and the chattering phenomenon. The disturbance rejection property depends upon the the switching gain. For example, for smaller values of the switching gain, the disturbance rejection property is poor. For increased values of the switching gain, the disturbance rejection property improves, but at the same time the system offers increased chattering [13].

In [14], an adaptive Lyapunov stability theory based nonlinear backstepping control strategy has been proposed for MPPT of a variable speed utility grid-connected PMSG-WECS. The robustness of the proposed paradigm was guaranteed without the prior knowledge of the upper bound of the uncertainties. The backstepping strategy is based on a recursive control design, in which the principal idea is the stabilization of the virtual control state [15]. Its attractive features include: fast dynamic response, robustness to system parametric uncertainties, good performance against unmodeled system dynamics and external disturbance rejection. It

is based on designing an MPPT controller recursively by choosing some of the system state variables as the virtual controllers, and then designing intermediate control laws for each of the selected virtual controller. This approach is well-suitable for boundary control problems. While the control is acting only from the boundary, its main feature is the capability of canceling out all the destabilizing effects (i.e. forces or terms) appearing throughout the domain [16, 17]. It does not employ model reduction. For finite dimensional nonlinear systems, the backstepping control serves as an extension of the feedback linearization control. Contrary to the standard feedback linearization control, the backstepping approach allows the flexibility to not necessarily cancel out the nonlinearity. Because, a nonlinearity may be retained if it is useful, or it may be dominated (rather than canceled nonrobustly) if it is potentially harmful and uncertain.

To overcome the stated problems with the standard ISMC, in this research article a nonlinear neuro-adaptive backstepping integral sliding mode control (NABISMC) based MPPT strategy is formulated for a standalone, variable speed, fixed-pitch, 3 kW PMSG-WECS. The proposed paradigm is a hybrid of the conventional backstepping and the ISMC schemes and its effectiveness is guaranteed through numerical simulations carried out in Matlab/Simulink under a stochastic wind speed profile. Further validation is guaranteed by giving a detailed performance comparison analysis of the proposed MPPT control strategy with the conventional feedback linearization control (FBLC), proportional integral derivative control (PID), sliding mode control (SMC) and the standard neuro-adaptive integral sliding mode control (NAISMC) based MPPT strategies, where the proposed strategy is found superior to the stated MPPT strategies in terms of offering more accurate MPPT, lower steady state error, faster dynamic response and lesser chattering.

This article is organized as follows: Section 2 presents the mathematical modeling of the variable speed, standalone, fixed-pitch PMSG-WECS. Section 3 covers the system coordinates transformation. Section 4 describes the system Lie derivatives estimation via the artificial neural network (ANN). Section 5 presents the proposed NABISMC based MPPT control design. Section 6 describes the performance evaluation of the proposed MPPT paradigm through Matlab simulations. Finally, Section 7 concludes this article.

2. Mathematical modeling of the variable speed standalone PMSG-WECS

A schematic of the overall variable speed, standalone, fixed-pitch, PMSG-WECS is illustrated in Figure 1. The main components of this system include: variable speed wind turbine (VSWT), gear-box, a PMSG coupled with the VSWT, power electronic converter and load.

2.1. Wind turbine modeling

A wind turbine, with fixed-pitch, can be described by the following group of mathematical equations [18, 19]:

$$\begin{aligned}
 P_m &= T_m \Omega_l = 0.5 \rho \pi R_t^2 v_w^3 C_p(\lambda, \beta) \\
 T_m &= \frac{P_m}{\Omega_l} = 0.5 \rho \pi R_t^3 v_w^2 C_T(\lambda) \\
 \lambda &= \frac{\Omega_l R_t}{v_w} \\
 C_p &= C_T(\lambda) \lambda \\
 \Omega_h &= \Omega_l i
 \end{aligned} \tag{1}$$

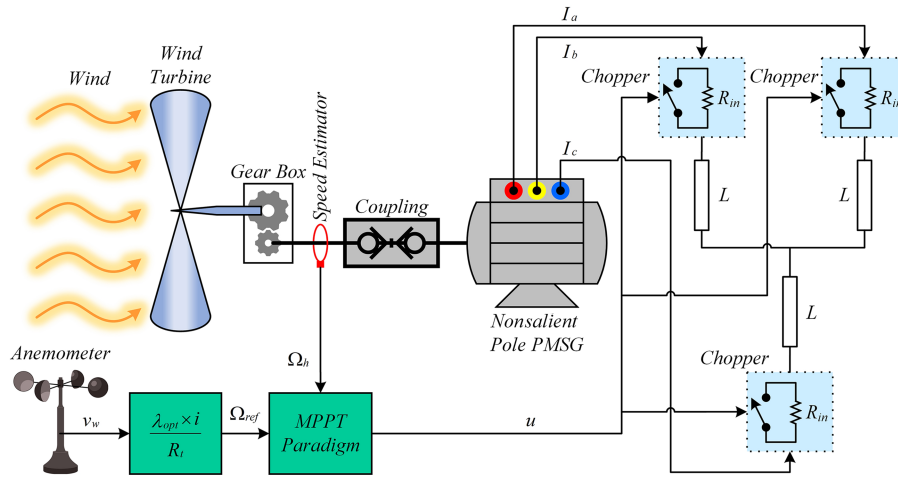


Figure 1. Schematic of the variable speed, standalone, PMSG-WECS.

where P_m represents the mechanical power developed (or captured) by the wind turbine, ρ indicates the air density (normally, 1.25 kg/m^3 , at 10°C , at sea level), R_t denotes the wind turbine blade radius (m), v_w represents the wind speed (m/s), C_p indicates the wind turbine rotor efficiency (or power conversion coefficient), C_T indicates the wind turbine torque coefficient, λ denotes the tip speed ratio (TSR), β indicates the turbine blade pitch angle (assumed to be a constant in this article, that is, $\beta = 0^\circ$), T_m stands for the wind turbine mechanical torque (N.m), Ω_h indicates the PMSG (high speed shaft) rotational speed (rad/s), Ω_l indicates the wind turbine (low speed shaft) rotational speed (rad/s), and i represents the gear ratio (or transmission ratio).

In a conventional WECS, if the wind speed exceeds beyond the nominal value, the pitch angle control strategy is implemented to limit the wind turbine mechanical power output and to ensure system safety. Since, the focus of this article is on the MPPT, hence, in this article it is assumed that the wind speed does not exceed the nominal value. Furthermore, the wind turbine blade pitch angle is always assumed to be fixed (or constant at $\beta = 0^\circ$) during the MPPT mode [20].

Generally, C_p varies proportionally with both λ , and β . But, in the MPPT mode (with $\beta = 0^\circ$), C_p is determined by numerical approximation. Such as, in [21], for $\beta = 0^\circ$, its approximate value is given by the following expression:

$$C_p(\lambda) = 0.0061\lambda - 0.0013\lambda^2 + 0.0081\lambda^3 - 9.7477 \times 10^{-4}\lambda^4 - 6.5416 \times 10^{-5}\lambda^5 + 1.3027 \times 10^{-6}\lambda^6 - 4.54 \times 10^{-7}\lambda^7 \quad (2)$$

C_p exhibits a unique maximum value (say, $C_{p_{max}}$) at a particular TSR, known as λ_{opt} . Hence, a VSWT continuously tracks the $C_{p_{max}}$, while maintaining the TSR at its optimal value, λ_{opt} , for the maximum wind power extraction.

C_T can also be found from a second-order polynomial expression, as a function of the TSR, as follows:

$$C_T(\lambda) = \alpha_0 + \alpha_1\lambda + \alpha_2\lambda^2 \quad (3)$$

Now, substituting λ from (1) and C_T from (3) in the wind turbine mechanical torque expression, T_m ,

given in (1), the resultant expression is as follows:

$$T_m = d_1 v_w^2 + \frac{d_2 v_w \Omega_h}{i} + \frac{d_3 \Omega_h^2}{i^2} \tag{4}$$

where,

$$\begin{cases} d_1 = 0.5\pi\rho R_t^3 \alpha_0, & d_2 = 0.5\pi\rho R_t^4 \alpha_1, & d_3 = 0.5\pi\rho R_t^5 \alpha_2 \\ \alpha_0 = 0.1253, & \alpha_1 = -0.0047, & \alpha_2 = -0.0005 \end{cases}$$

Different significant parameters of the wind turbine are expressed in Table . Once $C_{p_{max}}$ and λ_{opt} are known, the optimal mechanical power, $P_{m_{opt}}$, developed by the wind turbine can be obtained from (1), by substituting λ_{opt} , as follows:

$$P_{m_{opt}} = \frac{\rho\pi R_t^5 \Omega_l^3 C_{p_{max}}(\lambda)}{2\lambda_{opt}^3} \tag{5}$$

Table . Parameters of PMSG-WECS and MPPT controller.

Name	Parameters	Symbols	Values
Wind turbine	Air density (at sea level, at 0°C)	ρ	1.25 kg/m ³
	Wind turbine blade radius	R_t	2.5 m
	Maximum power conversion coefficient	$C_{p_{max}}$	0.4762
	Optimal tip speed ratio	λ_{opt}	7
	Average wind speed	$v_{w_{avg}}$	7 m/s
	Gear (or transmission) ratio	i	7
PMSG	Stator resistance	R_s	3.30 Ω
	Stator d, q -axis inductances	L_d, L_q	41.56 mH, each
	Magnetic flux	Φ_m	0.4382 Wb
	Number of pole pairs	p	3
	PMSG shaft inertia	J_h	0.055 22 kg m ²
	Load inductance	L_{ch}	0.08 H
	Initial chopper equivalent resistance	R_{ch}	80 Ω
NABISMC	Gain	k_2	0.1
	Gain	k_b	700
	Gain	k_i	2
	Gain	k_p	100
	Gain	k_q	0.001

Figure 2 illustrates the mechanical power developed by the wind turbine under different wind speeds. It can be seen that there exists a unique maximum power point, $P_{m_{opt}}$, at each wind speed. Collectively, these maximum power points constitute an optimal regime characteristic (ORC). The ORC corresponds to a region of operation, where the maximum energy can be extracted from the WECS under a fluctuating wind speed. The main function of the MPPT control strategy is to keep operating the wind turbine on the ORC, despite changes in the wind speed.

The optimal mechanical torque developed by the wind turbine, $T_{m_{opt}}$, can be deduced from the optimal

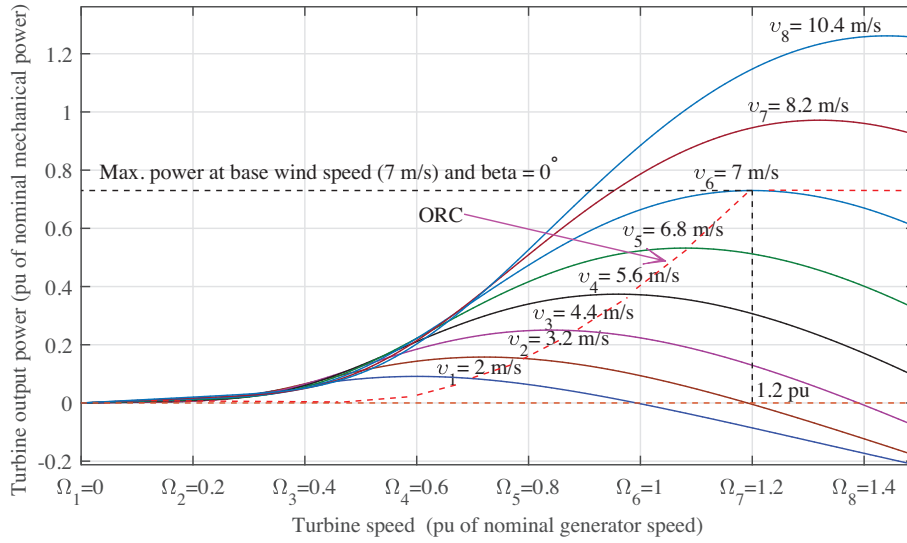


Figure 2. Mechanical power output of the wind turbine under different wind speeds.

mechanical power, $P_{m_{opt}}$ given in (5), as follows:

$$T_{m_{opt}} = \frac{P_{m_{opt}}}{\Omega_{\ell}} = \frac{\rho \pi R_t^5 \Omega_t^2 C_{p_{max}}(\lambda)}{2 \lambda_{opt}^3} \quad (6)$$

2.2. Permanent magnet synchronous generator modeling

The PMSG can be modeled in the dq -reference frame, where the zero components are neglected. For a standalone PMSG-WECS, the voltages on the dq -axes are regarded as the output variables. Using this concept, the PMSG model in terms of the dq -axes voltages can be expressed by the following set of differential equations [22]:

$$\begin{aligned} (L_d + L_{ch}) \frac{di_d}{dt} &= -(R_s + R_{ch}) i_d + p(L_q - L_{ch}) i_q \Omega_h \\ (L_q + L_{ch}) \frac{di_q}{dt} &= -(R_s + R_{ch}) i_q - p(L_d + L_{ch}) i_q \Omega_h + p\Phi_m \Omega_h \\ J_h \frac{d\Omega_h}{dt} &= \frac{T_m}{i} - T_{em} = \frac{T_m}{i} - [p(L_d - L_q) i_d i_q + p\Phi_m i_q] = \frac{d_1 v_w^2}{i} + \frac{d_2 v_w \Omega_h}{i^2} + \frac{d_3 \Omega_h^2}{i^3} - p\Phi_m i_q \end{aligned} \quad (7)$$

where L_d and L_q represent the stator d - and q -axis inductances, respectively, R_s is the stator resistance, i_d and i_q represent the stator d - and q -axis currents, respectively, p indicates the number of pole pairs, Φ_m is the maximum value of magnetic flux, T_{em} represents the electromagnetic torque of the PMSG, J_h denotes the moment of inertia of the PMSG (high speed shaft) and R_{ch} , L_{ch} indicate the resistance and inductance of the load, respectively. In (7), a nonsalient pole PMSG has been assumed, for which $L_d = L_q$.

Now, in state space representation, the PMSG-WECS model can be expressed as follows:

$$\underbrace{\begin{bmatrix} \dot{x}_1 \\ \dot{x}_2 \\ \dot{x}_3 \end{bmatrix}}_{\dot{\mathbf{x}}} = \underbrace{\begin{bmatrix} a_2x_1 + a_3x_2x_3 \\ b_2x_2 + b_3x_1x_3 + b_4x_3 \\ \frac{1}{J_h} \left(\frac{d_1v_w^2}{i} + \frac{d_2v_wx_3}{i^2} + \frac{d_3x_3^2}{i^3} - p\Phi_m x_2 \right) \end{bmatrix}}_{f(x)} + \underbrace{\begin{bmatrix} -\frac{x_1}{a_1} \\ -\frac{x_2}{b_1} \\ 0 \end{bmatrix}}_{g(x)} \cdot \underbrace{R_{ch}}_u y = \underbrace{\Omega_h}_{h(x)} \quad (8)$$

where $\mathbf{x} = [x_1 \ x_2 \ x_3]^T = [i_d \ i_q \ \Omega_h]^T \in \mathbb{R}^n$ represents the state vector, $f(x)$ and $g(x)$ indicate the nonlinear smooth vector fields, while u and y represent the control input and output, respectively. Moreover,

$$\begin{cases} a_1 = L_d + L_{ch}; & a_2 = -\frac{R_s}{a_1}; & a_3 = \frac{p(L_q - L_{ch})}{a_1} \\ b_1 = L_q + L_{ch}; & b_2 = -\frac{R_s}{b_1}; & b_3 = -\frac{p(L_d + L_{ch})}{b_1}; & b_4 = \frac{p\Phi_m}{b_1} \end{cases}$$

Different significant parameters of the PMSG are expressed in Table .

3. System coordinates transformation

Before expressing the system in standard canonical form (input-output form or normal form), the system coordinates transformation needs to be carried out. This coordinates transformation is carried out as follows:

$$z_1 = h(x) = x_3 = \Omega_h z_2 = L_f h(x) = \frac{\partial h(x)}{\partial x} f(x) = \gamma_1 v_w^2 + \gamma_2 v_w x_3 + \gamma_3 x_3^2 - \gamma_4 x_2 z_3 = a_3 \frac{x_1}{x_2} \quad (9)$$

where $\gamma_1 = \frac{d_1}{J_h i}$, $\gamma_2 = \frac{d_2}{J_h i^2}$, $\gamma_3 = \frac{d_3}{J_h i^3}$ and $\gamma_4 = d_4 = p\Phi_m$

As, the system under study has a relative degree, $r < n$ (system order), with $r = 2$, and $n = 3$, it means that the system can only be partially linearized. Furthermore, the standard canonical form can now be given as follows:

$$\dot{z}_1 = z_2 \dot{z}_2 = L_f^2 h(x) + L_g L_f h(x) u \quad (10)$$

where $L_f^2 h(x)$ and $L_g L_f h(x)$ are the system Lie derivatives. The overall closed loop PMSG-WECS control system is illustrated in Figure 3.

4. Artificial neural network configuration for system Lie derivatives estimation

Figure 4 represents a multilayer feedforward artificial neural network (ANN) configuration for system Lie derivatives estimation. This ANN has three layers, namely a hidden layer, an input layer and an output layer. It has four inputs which are z_1, z_2, z_3, v_w , while its two estimated outputs are $\hat{L}_f^2 h(x)$ and $\hat{L}_g L_f h(x)$. The targets are continuously updated until the error reaches an acceptable range. The hidden layer contains nine neurons, while the output layer contains two neurons that yields estimated outputs $\hat{L}_f^2 h(x)$ and $\hat{L}_g L_f h(x)$.

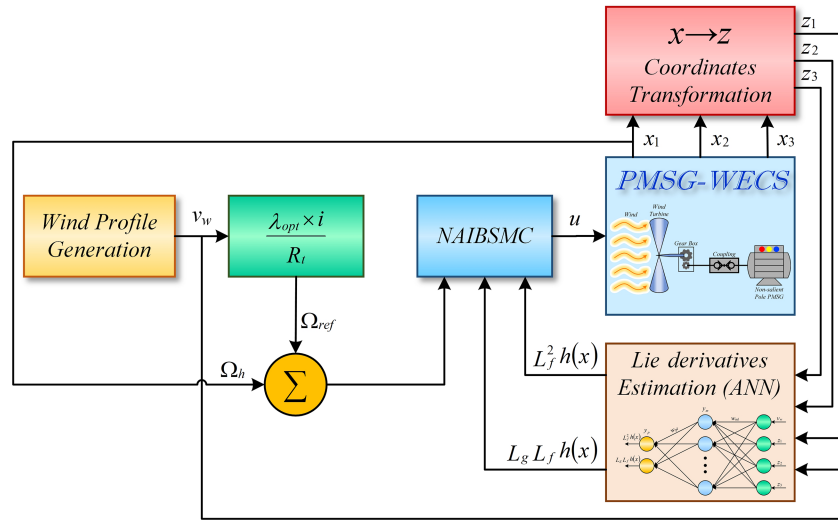


Figure 3. The overall closed loop PMSG-WECS control system.

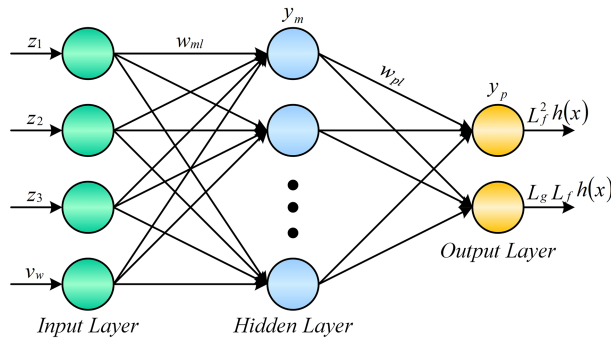


Figure 4. Artificial neural network configuration for system Lie derivatives estimation.

The input layer neurons provide input information to the hidden layer neurons, which in turn provide it to the output layer neurons, which then estimate the outputs $\hat{L}_f^2 h(x)$ and $\hat{L}_g L_f h(x)$. Tansigmoid activation function is used in the hidden layer, while a purelin function is used in the output layer. The ANN is trained using backpropagation algorithm. An input vector, $\psi = [z_1, z_2, z_3, v_w]^T$ is applied to the input layer neurons of the network, as illustrated in Figure 4.

The estimated output of the output layer neurons is expressed as follows:

$$y_p = f_0 \left[\sum_{m=1}^9 (w_{pm} y_m + b_p) \right] \tag{11}$$

As depicted in Figure 4, y_p has two values either $\hat{L}_f^2 h(x)$ or $\hat{L}_g L_f h(x)$. The weights adjustment expression is given as follows:

$$w_{ml}(n + 1) = w_{ml}(n) - \beta \left(\frac{\partial E_0}{\partial w_{ml}(n)} \right) + \zeta \Delta w_{ml}(n) \tag{12}$$

with

$$\Delta w_{ml}(n) = w_{ml}(n) - w_{ml}(n - 1) \quad (13)$$

where ζ , β are the momentum and learning factors, respectively.

5. Proposed NABISMC based MPPT control system design

To overcome the drawbacks of the standard ISMC stated in Section 1, an NABISMC based MPPT strategy is devised in this article for a variable speed, standalone, fixed-pitch, 3 kW PMSG-WECS.

In the proposed MPPT control design, the estimated values of the system Lie derivatives will be used for which the standard canonical form expressed in (10) can be rewritten as follows:

$$\dot{z}_1 = z_2 \dot{z}_2 = \widehat{L}_f^2 h(x) + \widehat{L}_g L_f h(x) u \quad (14)$$

where $u \in \mathbb{R}^n$ is the control variable, while $\widehat{L}_f^2 h(x)$ and $\widehat{L}_g L_f h(x)$ represent the estimated Lie derivatives of the system.

The following steps explain the designing of the proposed NABISMC algorithm:

Step 1: First of all, define a tracking error, along with its time-derivative, as follows:

$$e_1 = z_1 - z_{ref} \dot{e}_1 = \dot{z}_1 - \dot{z}_{ref} \quad (15)$$

where $z_{ref} = \Omega_{ref}$ is the desired (or reference) speed of the PMSG.

Step 2: Based on the standard ISMC, the proposed control law (NABISMC) is defined as follows:

$$u = u_i + u_d \quad (16)$$

where u_i represents the ideal control that can be designed using the linear feedback control law. On the other hand, u_d represents the discontinuous control that can be designed using the backstepping design approach.

Now, using the linear feedback control law, u_i can be designed as follows:

$$u_i = -k_b(e_1) - k_i(e_2) \quad (17)$$

Step 3: Next, design u_d based on the backstepping approach, as follows:

Since, the goal is to converge the tracking error, e_1 , asymptotically to the origin, O, (equilibrium point), for this purpose, selecting a suitable Lyapunov function candidate, $V_1(e_1)$. In order to ensure the asymptotic stability of the system, $V_1(e_1)$ must satisfy the following three conditions: (i) It must be positive definite, (ii) It must be radially unbounded, and (iii) It must have a negative definite time-derivative.

The selected Lyapunov function candidate, $V_1(e_1)$, is defined as follows:

$$V_1(e_1) = \frac{1}{2} e_1^2 \quad (18)$$

Differentiating (18) with respect to time and simplifying using (15), it yields:

$$\dot{V}_1 = e_1 \dot{e}_1 = e_1(\dot{z}_1 - \dot{z}_{ref}) = e_1(z_2 - \dot{z}_{ref}) \quad (19)$$

Now, considering z_2 in (19) as a virtual controller that acts as a stabilization function and it can be expressed as follows:

$$z_2^* = -k_2 e_1 + \dot{z}_{ref}$$

with $k_2 > 0$, (19) yields:

$$\dot{V}_1 = -k_2 e_1^2 < 0 \quad (20)$$

which is globally asymptotically stable.

Step 4: Next, define the ISMC sliding surface, as follows [23]:

$$s_1 = \sigma_i + z_i = (z_2 - z_2^*) + z_i = z_2 + k_2 e_1 - \dot{z}_{ref} + z_i \quad (21)$$

where z_i is the integral term.

Differentiating the sliding surface expressed in (21) and simplifying using (14) and (16), it yields:

$$\dot{s}_1 = \dot{z}_2 + k_2 \dot{e}_1 - \ddot{z}_{ref} + \dot{z}_i = \widehat{L}_f^2 h(x) + \widehat{L}_g L_f h(x) (u_i + u_d) + k_2 \dot{e}_1 - \ddot{z}_{ref} + \dot{z}_i \quad (22)$$

Now, selecting

$$\dot{z}_i = -\widehat{L}_g L_f h(x) u_i + \ddot{z}_{ref} \quad (23)$$

Substituting \dot{z}_i from (23) in (21), it yields:

$$\dot{s}_1 = \widehat{L}_f^2 h(x) + \widehat{L}_g L_f h(x) u_d + k_2 \dot{e}_1 \quad (24)$$

Step 5: Define a composite Lyapunov function candidate, $V_2(e_1, s_1)$, as follows:

$$V_2(e_1, s_1) = \frac{1}{2} (e_1^2 + s_1^2) \quad (25)$$

Taking the time derivative of (25), and simplifying using (19) it yields:

$$\dot{V}_2 = (e_1 \dot{e}_1 + s_1 \dot{s}_1) = \dot{V}_1 + s_1 \dot{s}_1 \quad (26)$$

Now, taking the reaching law as follows [24]:

$$\dot{s}_1 = (-k_p s_1 - k_q \text{sign}(s_1)) \quad (27)$$

Substituting (27) in (26), it yields:

$$\dot{V}_2 = (e_1 \dot{e}_1 + s_1 \dot{s}_1) = \dot{V}_1 + s_1 (-k_p s_1 - k_q \text{sign}(s_1)) \quad (28)$$

For asymptotic stability of the system, the time derivative of the composite Lyapunov function candidate, \dot{V}_2 , must be negative definite.

Now, equating (24) and (27), it yields:

$$-k_p s_1 - k_q \text{sign}(s_1) = \widehat{L}_f^2 h(x) + \widehat{L}_g L_f h(x) u_d + k_2 \dot{e}_1 \quad (29)$$

Hence, the discontinuous control law, u_d , can be expressed as follows:

$$u_d = \frac{-1}{\widehat{L}_g L_f h(x)} \left[\widehat{L}_f^2 h(x) + k_2 \dot{e}_1 + k_p s_1 + k_q \text{sign}(s_1) \right] \quad (30)$$

Finally, the overall proposed NABISMC law is obtained by substituting u_i and u_d from (17) and (30), respectively, in (16), as follows:

$$u_{NABISMC} = \underbrace{\frac{-1}{\widehat{L}_g L_f h(x)} \left[\widehat{L}_f^2 h(x) + k_2 \dot{e}_1 + k_p s_1 + k_q \text{sign}(s_1) \right]}_{u_d} \underbrace{-k_b(e_1) - k_i(e_2)}_{u_i} \quad (31)$$

Different parameters of the NABISMC law are given in Table , whereas the computational flow chart for its implementation is illustrated in Figure 5.

6. MPPT paradigm performance evaluation through numerical simulations

This section validates the performance and effectiveness of the proposed nonlinear NABISMC based MPPT scheme, through various numerical simulations carried out in Matlab/Simulink. The conventional FBLC, PID, SMC and the standard NAISMC based MPPT schemes have been chosen as benchmarks to manifest the superior performance of the proposed MPPT strategy. The wind speed is assumed to have a stochastic profile with frequent and rapid wind speed fluctuations throughout the simulations.

Figures 3 and 5 illustrate the implementation of the proposed nonlinear MPPT control scheme to the variable speed, standalone, fixed-pitch, 3 kW PMSG-WECS. The maximum power conversion coefficient, $C_{p_{max}} = 0.4762$ is computed from (2) that occurs at an optimal tip speed ratio, $\lambda_{opt} = 7$. All the simulations are carried out for 100 s horizon with an average wind speed of, $v_{w_{av}} = 7$ m/s (illustrated in Figure 2). The MPPT scheme keeps the tip speed ratio, λ , at its optimal value, λ_{opt} , thus ensuring the maximum power extraction from the PMSG-WECS.

Figure 6 illustrates the PMSG rotational speed tracking performance, where the zoomed-in segments of the figure clearly reveal that the the proposed NABISMC based MPPT strategy renders a superior PMSG speed tracking performance to all the other MPPT candidates. The superior performance of the the proposed strategy is further validated by the PMSG speed tracking error, as depicted in Figure 7. It is evident that the proposed paradigm renders the minimum tracking error and minute chattering. Figures 8 and 9 indicate the TSR and the power conversion coefficient evolution. The proposed MPPT strategy much accurately maintains the TSR at $\lambda_{opt} = 7$ and $C_{p_{max}} = 0.4762$, that is an indication of the maximum wind power extraction, with minute chattering. Figures 10 and 11 illustrate the wind turbine and the PMSG mechanical powers development against the TSR. The proposed MPPT paradigm much precisely maintains the TSR around its optimal value, λ_{opt} , than the other MPPT benchmarks. The wind turbine mechanical power evolution against its rotational speed is depicted in Figure 12. It can easily be concluded that the proposed MPPT algorithm much accurately keeps operating the WECS in the ORC and ensures the maximum power extraction from it. Similarly, Figure 13 shows the PMSG electromagnetic torque development against the TSR. Again, the proposed MPPT strategy

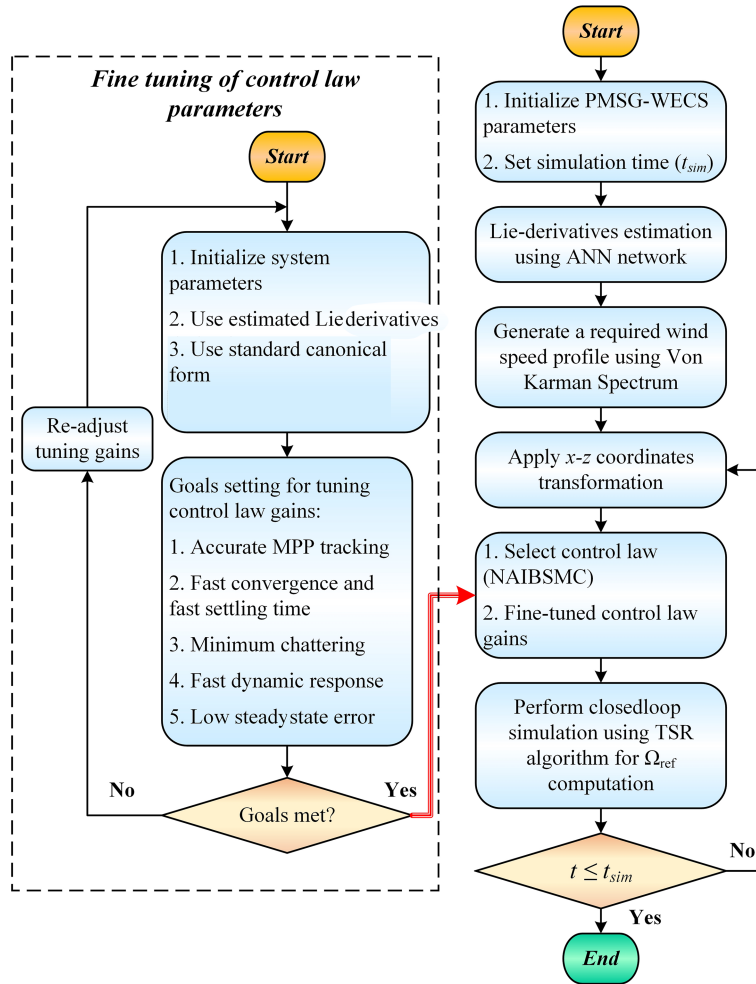


Figure 5. Computational flow chart for implementation of the proposed MPPT control algorithm.

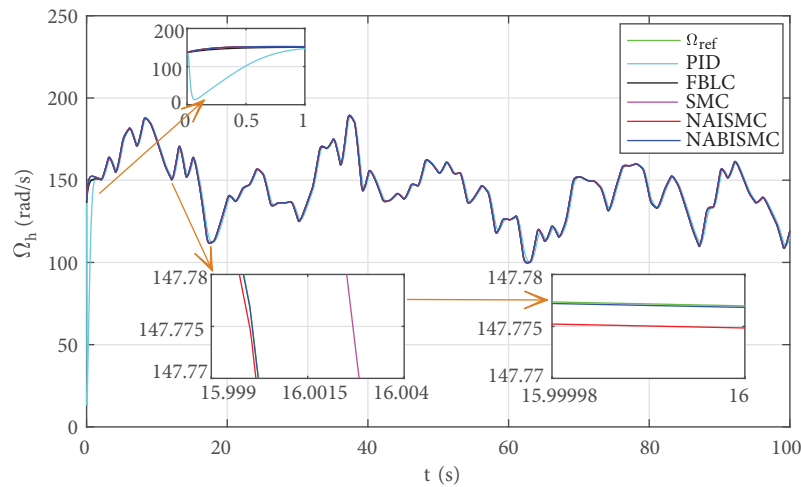


Figure 6. PMSG speed tracking performance.

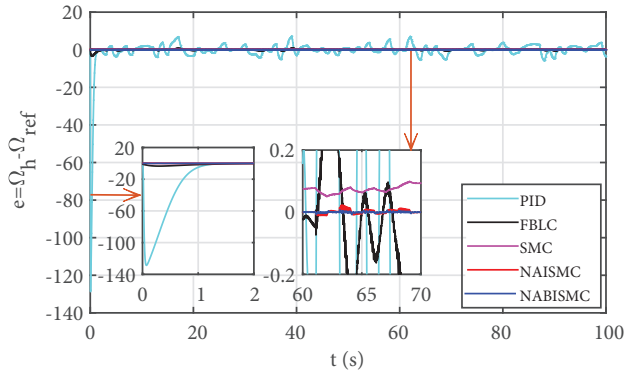


Figure 7. PMSG speed tracking error.

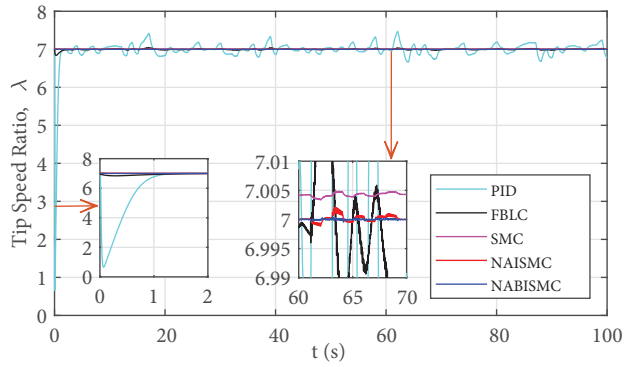


Figure 8. Tip speed ratio evolution.

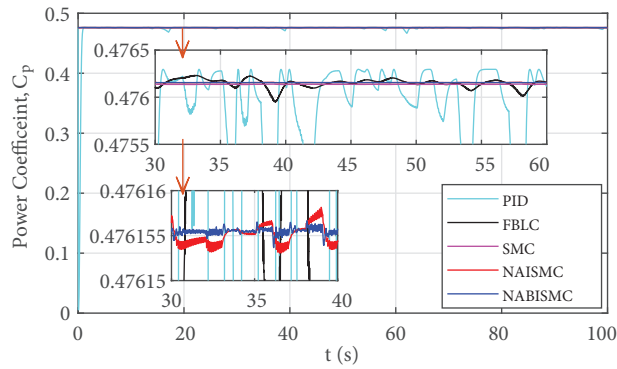


Figure 9. Power conversion coefficient evolution.

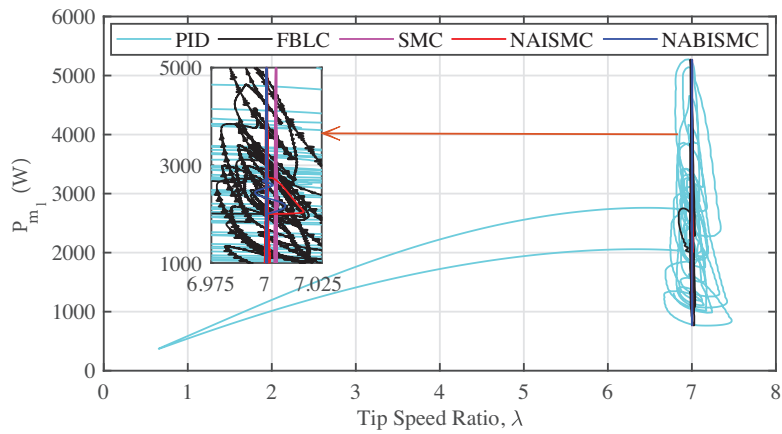


Figure 10. Wind turbine mechanical power vs. the tip speed ratio.

is capable of keeping the TSR around its optimal value, thereby ensuring the maximum power extraction from the WECS.

To supplement the superior performance of the proposed NABISM based MPPT paradigm against the FBLC, PID, SMC and NAISM based MPPT benchmarks, the dynamic performance of all the stated MPPT

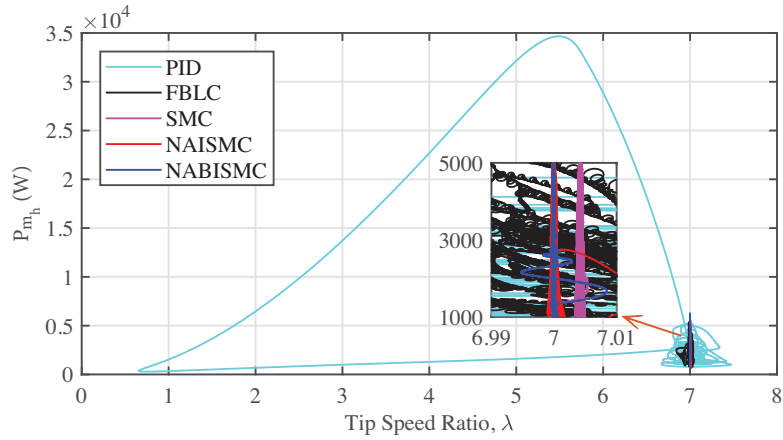


Figure 11. PMSG mechanical power vs. the tip speed ratio.

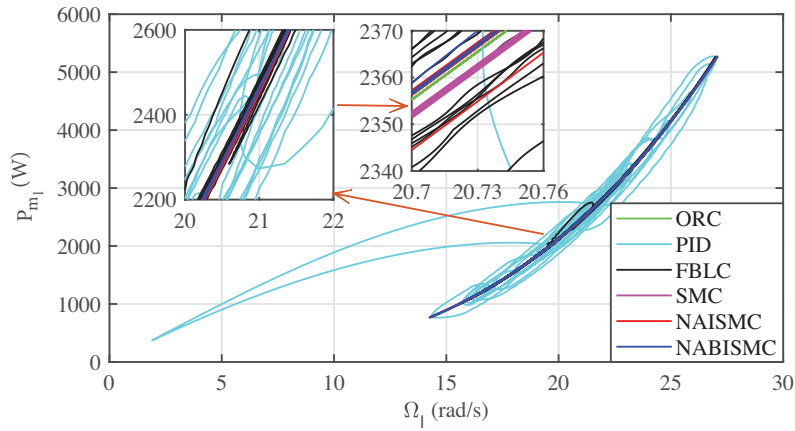


Figure 12. Wind turbine mechanical power vs. shaft speed.

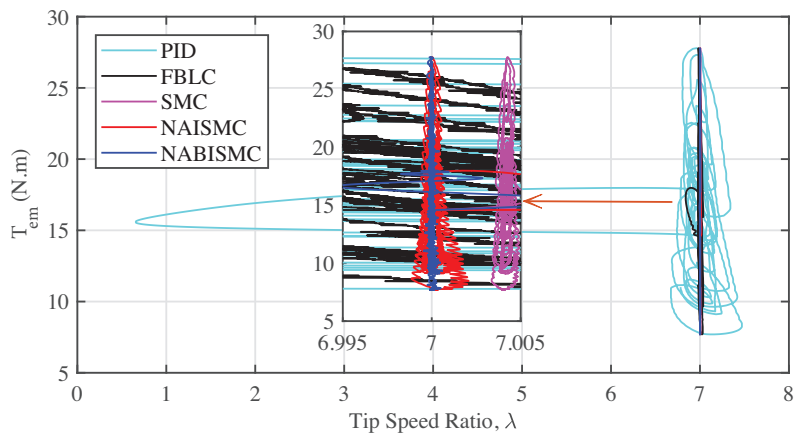


Figure 13. PMSG electromagnetic torque vs. the tip speed ratio.

candidates is also evaluated using four different well-known performance indices, expressed as follows [25–27]:

$$ISE = \int_0^{t_{sim}} [e(t)]^2 dt, ITSE = \int_0^{t_{sim}} t [e(t)]^2 dt, IAE = \int_0^{t_{sim}} |e(t)| dt, ITAE = \int_0^{t_{sim}} t |e(t)| dt \quad (32)$$

where $e(t) = \Omega_h - \Omega_{ref}$ and t_{sim} represents the total simulation time.

The performances indices, *ISE* (integral squared error), *ITSE* (integral of time squared error), *IAE* (integral absolute error), and *ITAE* (integral of time absolute error) have been computed for PMSG-WECS using (32) for all the MPPT candidates, and have been compared in Figures 14-17. It can be seen that as the time advances, the accumulative error of each MPPT scheme also increases. Nonetheless, the proposed NABISMC based MPPT paradigm renders a smoother, more flat and smaller error profile than all the other MPPT benchmarks, thus validating its superior performance.

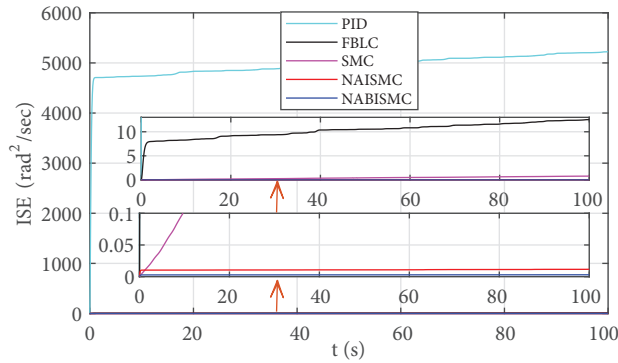


Figure 14. Integral squared error.

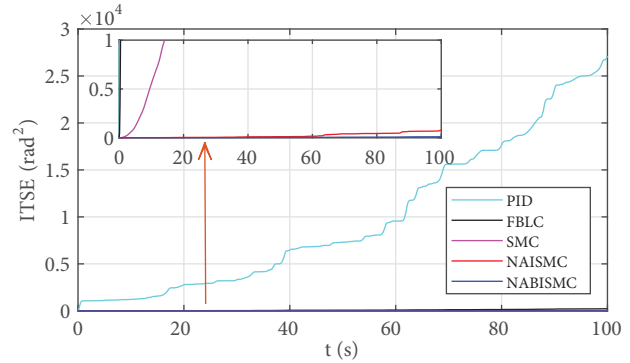


Figure 15. Integral of time squared error.

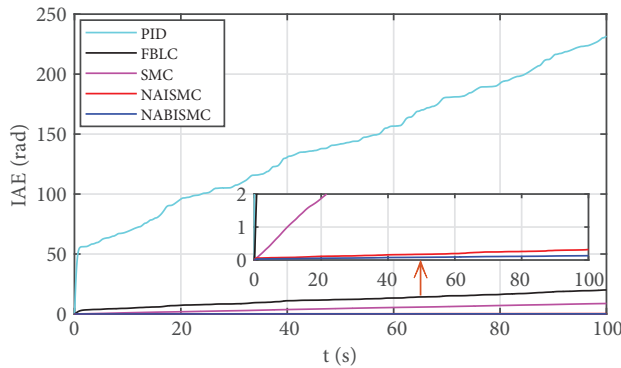


Figure 16. Integral absolute error.

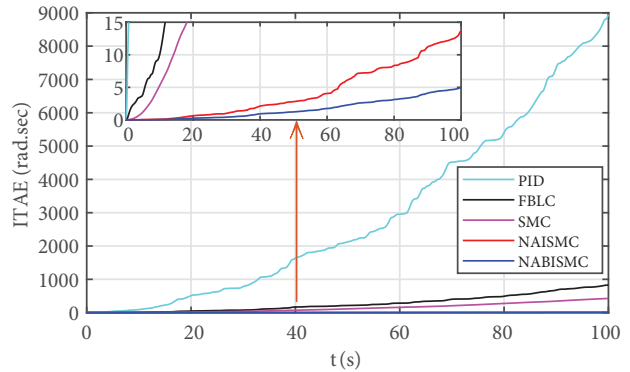


Figure 17. Integral of time absolute error.

7. Conclusion

Because of the randomness and instability of the wind speed, the WECS is a complex nonlinear uncertain system. Consequently, the MPPT control for PMSG-WECS is a challenging problem. To deal with the inconsistent wind speed and to optimize the power extraction from the PMSG-WECS, in this article, a nonlinear NABISMC based MPPT strategy has been proposed for a 3 kW, variable speed, fixed-pitch, standalone PMSG-WECS. The proposed paradigm was a hybrid of the conventional backstepping and the ISMC based MPPT schemes that has been simulated and tested under a stochastic wind speed profile in Matlab/Simulink, and its performance has been found superior to the conventional FBLC, PID, SMC and the standard NAISMC based MPPT strategies in terms of offering more accurate MPPT, lower steady state error, faster dynamic response and lesser chattering.

Nomenclature

C_p	Wind turbine rotor power conversion coefficient (or efficiency)
C_T	Wind turbine torque coefficient
J_h	High speed shaft (PMSG) inertia
L_{ch}	Chopper inductance
L_d, L_q	Stator d and q – axes inductances
p	Number of pole pairs
P_m	Wind turbine mechanical power
R_{ch}	Chopper resistance
R_t	Wind turbine blade radius
R_s	Stator resistance
T_{em}	Electromagnetic torque
T_m	Wind turbine mechanical torque
v_w	Wind speed
β	Wind turbine blade pitch angle
Ω_h	PMSG speed (high speed shaft rotational speed)
Ω_l	Wind turbine speed (low speed shaft rotational speed)
ϕ_d, ϕ_q	Stator d - and q -axis magnetic fluxes
Φ_m	Magnetic flux due to permanent magnets
λ	Tip speed ratio (TSR)
ρ	Air density

References

- [1] Hamatwi E, Davidson IE, Gitau MN. Rotor speed control of a direct-driven permanent magnet synchronous generator-based wind turbine using phase-lag compensators to optimize wind power extraction. *Journal of Control Science Engineering* 2017; 1: 1-17. doi: 10.1155/2017/6375680
- [2] Tahir K, Belfedal C, Allaoui T, Denai M, Doumi, M. A new sliding mode control strategy for variable-speed wind turbine power maximization. *International Transactions on Electrical Energy Systems* 2018; 28 (4): e2513. doi: 10.1002/etep.2513
- [3] Yazici İ, Yaylaci EK. Maximum power point tracking for the permanent magnet synchronous generator-based WECS by using the discrete-time integral sliding mode controller with a chattering-free reaching law. *IET Power Electronics* 2017; 10 (13): 1751-1758. doi: 10.1049/iet-pel.2017.0232
- [4] Asri A, Mihoub Y, Hassaine S, Logerais PO, Allaoui T. Intelligent maximum power tracking control of a PMSG wind energy conversion system. *Asian Journal of Control* 2019; 21 (4): 1980-1990. doi: 10.1002/asjc.2090
- [5] Yaramasu V, Dekka A, Durán MJ, Kouro S, Wu B. PMSG-based wind energy conversion systems: survey on power converters and controls. *IET Electric Power Applications* 2017; 11 (6): 956-968. doi: 10.1049/iet-epa.2016.0799
- [6] Soliman MA, Hasanien HM, Azazi HZ, El-kholy EE, Mahmoud SA. Linear-quadratic regulator algorithm-based cascaded control scheme for performance enhancement of a variable-speed wind energy conversion system. *Arabian Journal for Science and Engineering* 2019; 44 (3): 2281-2293. doi: 10.1007/s13369-018-3433-6
- [7] Shtessel Y, Edwards C, Fridman L, Levant A. *Sliding Mode Control and Observation*. Birkhäuser, NY, USA: Springer, 2014.
- [8] Young KD, Utkin VI, Ozguner U. A control engineer's guide to sliding mode control. *IEEE Transactions on Control Systems Technology* 1999; 7 (3): 328-342. doi: 10.1109/87.761053
- [9] Coban R. Adaptive backstepping sliding mode control with tuning functions for nonlinear uncertain systems. *International Journal of Systems Science* 2019; 50 (8): 1517-1529. doi: 10.1080/00207721.2019.1615571

- [10] Coban R. Dynamical adaptive integral backstepping variable structure controller design for uncertain systems and experimental application. *International Journal of Robust and Nonlinear Control* 2017; 27 (18): 4522-4540. doi: 10.1002/rnc.3810
- [11] Aksu IO, Coban R. Sliding mode PI control with backstepping approach for MIMO nonlinear cross-coupled tank systems. *International Journal of Robust and Nonlinear Control* 2019; 29 (6): 1854-1871. doi: 10.1002/rnc.4469
- [12] Utkin V, Sh J. Integral sliding mode in systems operating under uncertainty conditions. In: *Proceedings of 35th IEEE Conference on Decision and Control*; New York, NY, USA; 1996. pp. 4591-4596. doi: 10.1109/CDC.1996.577594
- [13] Xia, C, Wang X, Li S, Chen X. Improved integral sliding mode control methods for speed control of PMSM system. *International Journal of Innovative Computing, Information and Control* 2006; 7: 1971-1982.
- [14] Wang J, Bo D, Ma X, Zhang Y, Li Z et al. Adaptive back-stepping control for a permanent magnet synchronous generator wind energy conversion system. *International Journal of Hydrogen Energy* 2019; 44 (5): 3240-3249. doi: 10.1016/j.ijhydene.2018.12.023
- [15] Errami Y, Obbadi A, Sahnoun S, Benhmida M, Ouassaid M et al. Design of a nonlinear backstepping control strategy of grid interconnected wind power system based PMSG. In: *AIP Conference Proceedings*; Beirut, Lebanon; 2016. pp. 030053.
- [16] Krstić M, Kanellakopoulos I, Kokotović, PV. *Nonlinear and Adaptive Control Design*. USA: John Wiley & Sons Inc., 1995.
- [17] Krstić M, Smyshlyaev A. *Boundary Control of PDEs: A Course on Backstepping Designs*. Philadelphia, PA, USA: Siam (Society for Industrial and Applied Mathematics), 2008.
- [18] Cheikh R, Menacer A, Chrifi-Alaoui L, Drid S. Robust nonlinear control via feedback linearization and Lyapunov theory for permanent magnet synchronous generator-based wind energy conversion system. *Frontiers in Energy* 2018; 1: 1-12. doi: 10.1007/s11708-018-0537-3
- [19] Subramaniam R, Joo YH. Passivity-based fuzzy ISMC for wind energy conversion systems with PMSG. *IEEE Transactions on Systems, Man, and Cybernetics: Systems* 2019; 1: 1-10. doi: 10.1109/TSMC.2019.2930743
- [20] Heshmatian S, Khaburi DA, Khosravi Mahyar, Kazemi A. A control scheme for maximizing the delivered power to the load in a standalone wind energy conversion system. *Turkish Journal of Electrical Engineering and Computer Sciences* 2019; 27 (4): 2998-3014. doi: 10.3906/elk-1809-166
- [21] Munteanu I, Bratcu AI, Cutululis NA, Ceanga E. *Optimal Control of Wind Energy Systems: Towards a Global Approach*. London, UK: Springer-Verlag, 2008. doi: 10.1007/978-1-84800-080-3
- [22] Cutululis NA, Ceanga E, Hansen AD, Sørensen P. Robust multi-model control of an autonomous wind power system. *Wind Energy* 2006; 9 (5): 399-419. doi: 10.1002/we.194
- [23] Mat-Noh M, Arshad MR, Mohd-Mokhtar R, Khan Q. Back-stepping integral sliding mode control (BISMC) application in a nonlinear autonomous underwater glider. In: *IEEE 7th International Conference on Underwater System Technology: Theory and Applications (USYS)*; Kuala Lumpur, Malaysia; 2017. pp. 1-6.
- [24] Khan Q, Bhatti AI, Iqbal S, Iqbal M. Dynamic integral sliding mode for MIMO uncertain nonlinear systems. *International Journal of Control, Automation, and Systems* 2011; 9 (1): 151-160. doi: 10.1007/s12555-011-0120-8
- [25] Duman S, Yörükeren N, Altaş İH. Gravitational search algorithm for determining controller parameters in an automatic voltage regulator system. *Turkish Journal of Electrical Engineering and Computer Sciences* 2016; 24 (4): 2387-2400. doi: 10.3906/elk-1404-14
- [26] Ali K, Khan Q, Ullah S, Khan I, Khan L. Nonlinear robust integral backstepping based MPPT control for stand-alone photovoltaic system. *PLoS One* 2020; 15 (5): e0231749. doi: 10.1371/journal.pone.0231749
- [27] Sami I, Ullah S, Ali Z, Ullah N, Ro JS. A super twisting fractional order terminal sliding mode control for DFIG-based wind energy conversion system. *Energies* 2020; 13 (9): 2158. doi: 10.3390/en13092158